Unusual fluid of one-dimensional disordered bosons at finite temperature

Asaad R. Sakhel [1,*] William J. Mullin [2] and Roger R. Sakhel [3]

[1]*Department of Physics, Faculty of Science, Al-Balqa Applied University, Salt 19117, Jordan*
[2]*Department of Physics, Hasbrouck Lab, University of Massachusetts Amherst, Amherst, Massachusetts 01003, USA*
[3]*Department of Physics, Faculty of Science, Isra University, Amman 11622, Jordan*

In previous important examinations by Aleiner *et al.* [Nat. Phys. **6**, 900 (2010)] and Michal *et al.* [Proc. Natl. Acad. Sci. (U.S.A.) **113**, E4455 (2016)], the fluid insulator transition has been explored in one-dimensional (1D) disordered bosons by analytical methods. However, the nature of this "fluid" is still not quite understood. Here we shed more light on this "fluid" by studying its properties under changes in the average particle number $\langle N \rangle$ and temperature T in the absence of superfluidity. For this purpose, the worm algorithm path-integral Monte Carlo method is utilized in the grand-canonical ensemble. A measure for the width of path fluctuations is introduced that we call σ_J. It is found that by increasing $\langle N \rangle$, σ_J rises as the bosons become less repulsive and gain more mobility. The compressibility $\chi(\mu)$, μ being the chemical potential, reveals fluid behavior at the lower γ and a proposed Bose-glass phase at the larger γ (the Lieb-Liniger interaction parameter). The kinetic energy E_K versus γ at various T signals a transition by its convergence towards a common value. E_K versus μ reveals a peculiar inversion as one goes from small to larger values of the speckle strength $\langle V \rangle$ demonstrating a complex influence of the disorder. A tipover of E_K versus γ from an increasing to a decreasing trend at the lower γ also signals a transition. Further, Luttinger's liquid theory cannot be applied to describe 1D bosons in strong disorder at finite T because of the absence of superfluidity. Moreover, $\langle V \rangle$ largely controls the behavior of $\chi(\mu)$, the pair-correlation function at the origin $g_2(0)$, and E_K. Surprisingly, the diffusion constant D_0 does not obey the classical isomorphism as it rises with T. We also emphasize the importance of this work via its applicability to quantum wires.

I. INTRODUCTION

One-dimensional (1D) bosons in disorder have mostly been examined at ultracold temperatures [1–7], and phenomena such as the superfluid-insulator transition [8–16], finite-temperature phase transitions [17–20], and many-body localization in a quasirandom optical lattice [21] have been largely explored. The effect of disorder on a 1D Bose-Einstein condensate has also been investigated numerically [22]. See also the interesting review articles by Modugno [23] and Sanchez-Palenchia and Lewenstein [24]. Some of the earliest papers on the problem of 1D disordered Bose systems are quite remarkable. For example, Scalettar *et al.* [25] applied quantum Monte Carlo methods to explore the 1D disordered Bose system. They demonstrated the destruction of superfluidity by disorder and for the first time the emergence of a Bose-glass phase. Singh and Rokhsar [26] investigated the same system using real-space renormalization-group theory, and they found among other things that a Bose-glass phase intervenes between the superfluid and Mott-insulator phases. Zhang and Ma [27] studied a dirty 1D boson problem with hard-core interactions using the same method. It has been found that the superfluid state can be destroyed by strong disorder and becomes unstable against any finite amount of disorder. A new effect considered in the present work is that of the thermodynamic average particle number $\langle N \rangle$ and the role of its interplay with disorder in defining the properties of bosons in a random (speckle) potential of strength $\langle V \rangle$. In 1D homogeneous systems, it is known that $\langle N \rangle$ defines the interactions via the Lieb-Liniger parameter [18]

$$\gamma = -\frac{2}{n a_{\rm sc}}, \tag{1}$$

where $n = \langle N \rangle / L$ is the number density, L being the length of the system and $a_{\rm sc}$ the scattering length. Therefore, if $a_{\rm sc}$ is kept fixed, then $\gamma \propto 1/\langle N \rangle$, and $\langle N \rangle$ is expected to play a major role here in defining the properties. To this end, we assume an artificial γ that is only varied by changing $\langle N \rangle$. Presenting the study in terms of γ is very common and displays immediately the values of γ at which phase transitions can occur. In addition, our presentation in terms of γ instead of $\langle N \rangle$ is also just a matter of taste or preference. Furthermore, in a future investigation we would like to change $a_{\rm sc}$ while keeping $\langle N \rangle$ fixed. Plotting versus γ allows then a better comparison between the present results and future ones. Earlier [22], it was noted that in contrast to higher dimensions, a gas in 1D "can be made strongly interacting by lowering its density."

In a previous important examination, Aleiner *et al.* [18] and Michal *et al.* [17] studied the fluid insulator transition in a 1D disordered environment using analytical methods. However, the nature of the "fluid" in [17,18] is not quite understood.

*Corresponding author: asakhel@bau.edu.jo

It is identified as a fluid and not a superfluid, and whether it is a normal fluid remains to be determined. Thus the novelty of the present work lies in the fact that it aims to shed more light on this fluid by studying its properties under changes in particle number and temperature. Recently, Masella *et al.* [28] discovered an unusual conducting state of bosonic matter in disordered 1D chains of bosons in the absence of superfluidity. They called this unusual state an anti-Drude metal of bosons. It has been characterized by optical conductivity and could bear a resemblance to the "fluid" discussed in the present work. Their ground state has been determined using the worm algorithm method [29].

Hence, the main goal of this work is to understand the properties of the aforementioned "fluid," i.e., 1D disordered interacting bosons at finite temperature in the absence of superfluidity. It should be emphasized that strictly speaking in a 1D quantum system, superfluidity cannot exist at finite T and infinite length $L \to \infty$. Superfluidity in 1D at $T > 0$ is essentially a finite-size effect. This is evidenced as follows:

(a) Del Maestro and Affleck [30] computed the superfluid fraction in a 1D Bose gas at finite L and T in the framework of Luttinger liquid (LL) theory using the continuous-space worm algorithm path-integral Monte Carlo method (WAPIMC).

(b) Markić *et al.* [31] conducted an extensive study of a 1D Bose quantum liquid using diffusion Monte Carlo (DMC) and path integral Monte Carlo (PIMC) methods to test LL predictions for 1D fluids. The Bose fluid examined was a chain of ^{4}He atoms inside a narrow nanopore. The superfluid fraction ρ_s/ρ_0 has been evaluated at $T > 0$ at finite length L. Two types of ρ_s/ρ_0 have been reported: a "thermodynamic" arising from the evaluation of the PIMC winding number, and a "dynamical" obtained from phase twists over the length L of the system. The aforementioned authors particularly state the following:

"In 1D spinless Bose and Fermi fluids, low energy phenomena such as superflow and BEC is expected to follow the predictions of Luttinger liquid (LL) theory [···]. The OBDM is predicted to show a decaying algebraic tail at low temperature that has oscillations which extend to large distances reflecting the atomic order in 1D. The pair distribution function (PDF) has similar long-range oscillations. These oscillations are uniquely characteristic of 1D and are not seen in the OBDM or PDF in 2D or 3D fluids. Superfluidity in 1D is really only a finite size effect. There is no T_c. The ρ_s/ρ_0 has a characteristic 1D shape and scales as LT, the product of the temperature T and length L of the 1D system."

(c) Maestro *et al.* in another work [32] explored the low-T properties of a ^{4}He fluid confined in nanopores. It has been noted that the pore can be modeled as a long cylindrical cavity carved inside a continuous medium and that if the pore radius is small enough it should be possible to observe a crossover to strictly 1D behavior. In their Fig. 3, the pair correlation function signals the presence of a superfluid fraction in a nanopore of finite length. The superfluid fraction as a function of T is displayed as well. In their Ref. [20], it is noted that,

"The observed superfluid response is a finite-size effect, i.e., it vanishes in the $L \to \infty$ limit at fixed $T > 0$. However, LL theory provides a prediction for the superfluid fraction [···] which can be used to extract further information about $\nu = K$."

However, it should be emphasized that in the present finite-sized system, *global* superfluidity is absent because of the presence of a strong disorder potential, and not because the system is long enough or that the temperature is high.

We examine the fluid via the concept of path integrals (PIs). In PI math, classical behavior has a definite path, and quantum behavior has a zittering uncertain path that is quite irregular. At $T = 0$ in the ground state, whatever motion there is is zero-point and it has a wide zittering path as there are many possible classical paths that the quantum behavior can follow. A measure for the width of the PI fluctuations in a disordered environment and in the absence of superfluidity is therefore required. Thus in this work, we provide a measure for this width via a term that closely resembles the spring term of the kinetic energy in a PIMC formulation [33]. We refer to it as the measure for the width of path fluctuations (MWPF), and we call it σ_J. Further, we explore the dynamic susceptibility $\chi(\mu)$ (μ being the chemical potential), imaginary-time diffusion constant (ITDC) D_0, kinetic energy E_K, interaction energy E_{int}, and the second-order local correlation function $g_2(r = 0)$ at the origin. In terms of importance, $g_2(0)$ has been utilized to reveal fermionization [34], whereas $\chi(\mu)$ counts as an important quantity to detect a Bose glass [15,16,35,36] or a Mott-insulator such as in [37–40]. Moreover, D_0 measures the extent by which a particle propagates through a speckle potential. The above-mentioned quantities will help us in reaching a better understanding of the "fluid" as we observe their response to changes in $\langle N \rangle$ and temperature T.

The WAPIMC method [41] is applied to calculate the latter quantities numerically. This study is conducted in the grand-canonical ensemble, where the particle number is determined by, and allowed to change with, the chemical potential μ. It should be noted that the PIMC method does not make use of a wave function in the calculations, since PIMC is a many-body technique.

After evaluating the properties as functions of γ, T, and μ, the key results of this study turned out to be as follows: (a) The MWPF σ_J decreases with γ and declines with T heading towards an insulator. (b) D_0 displays a weaker response to γ and rises with increasing T. Further, D_0 seems surprisingly robust to changing γ. (c) $\chi(\mu)$ rises significantly as γ approaches zero; from this, one can infer the presence of a noninsulating state. $\chi(\mu)$ also declines in general with T heading again towards an insulating state. Moreover, $\chi(\mu)$ is likely to approach zero when $\gamma \to \infty$. (d) E_K reveals complex behavior with γ that varies with $\langle V \rangle$. In general, E_K rises with T, and this behavior is almost linear indicating the tendency towards classical behavior. (e) $g_2(0)$ displays also complicated behavior that differs largely with $\langle V \rangle$.

It turns out that $\chi(\mu)$ and E_K are good measures for the mobility of the bosons in disorder. From the above-mentioned results, the role of the interplay between the interactions and disorder can be inferred by defining the response of the system to changes in $\langle N \rangle$ and T.

In previous work with relevance to the present, Gori *et al.* [19] analyzed the finite-T effects on the phase diagram of interacting bosons in a 1D disordered lattice. In their work, the effective thermal correlation length has been used as a phenomenological parameter to quantify the loss of coherence due to an increase in T. It has been argued that a reduction of

this length can be indicative of a crossover from a quantum to a normal phase. According to Gori *et al.* [19], the quantum phases are the Mott insulator and the strongly interacting Bose glass. Michal *et al.* [42] showed that for a quasiperiodic potential at higher temperatures, stronger interactions are required to maintain delocalization and that an insulator can be obtained by heating. Gornyi *et al.* [43] found that the conductivity of electrons in a quantum wire revealed variable-range hopping character, and that at higher T one gets weak localization, whereas strong localization sets in at lower T. Chen *et al.* [44] have shown that for a Bose-Einstein condensate in a disordered optical potential, there is an inhibition of transport and a damping of dipole oscillations. The Gross-Pitaevskii equation in the presence of a disordered potential has also been applied [45–53]. A disorder-induced insulating state of strongly interacting fermions in an optical lattice has also been studied [54].

Other investigations have been directed towards how the conductivity behaves in a disordered Luttinger liquid [43,55], the temperature dependence of the conductivity [56–58], the interplay of disorder and interactions [45], and the behavior of the conductance as a function of interaction γ [59].

The remainder of this paper is organized as follows. In Sec. II, our view on the MWPF as applied here to 1D bosons in disorder is introduced along with some implications. In Sec. III, the applicability and importance of the present work is presented. In Sec. IV, we outline the method. In Sec. V, the results are displayed and discussed. In Sec. VI, the paper concludes with a future outlook.

II. MEASURE OF THE WIDTH OF PATH FLUCTUATIONS

The facts found in the above-mentioned literature on disordered bosons motivated us to seek an order parameter to measure their MWPF. We therefore found it convenient to formally define a quantity of the form

$$\sigma_J = \frac{1}{\tau_0}\left\langle \int_0^\beta \Delta(\tau)^2 d\tau \right\rangle, \tag{2}$$

where $\Delta(\tau)$ is the sum of the displacements of all particles between the times $\tau + \tau_0$ and τ, i.e.,

$$\Delta(\tau) = \sum_{i=1}^N [x_i(\tau + \tau_0) - x_i(\tau)]. \tag{3}$$

Here, $x_i(\tau)$ is the position of a particle "i" at imaginary-time τ, and τ_0 is a time step. The aforementioned integral (2) is formally in continuous time from $\tau = 0$ to some time β. In the present calculations, $\Delta(\tau)$ is evaluated in discrete time steps along the imaginary-time axis in a grand-canonical WAPIMC simulation, where $\beta = M\tau$ is the length of the path, i.e., the total time along M time slices. The $\langle \cdots \rangle$ indicates an average over all WAPIMC configurations. There is another quantity next to (2) that is related to the current-current correlations, namely

$$\int_0^\beta \langle \mathcal{T} J(\tau) J(0)\rangle d\tau, \tag{4}$$

which can be proven to be proportional to $\langle W^2 \rangle$, W being the winding number [60], and $\mathcal{T}$ is the time-ordering operator.

This is shown in Appendix E. However, in the absence of a superfluid fraction, $\langle W^2 \rangle = 0$, and therefore the above quantity (4) vanishes as well.

The present work bears some similarities to that of Batrouni and Scalletar (BS) [61], who applied a physical observable of the form

$$K(\tau) = \langle j(\tau) j(0)\rangle \tag{5}$$

with

$$j(\tau) = \sum_{i=1}^{N_b} \langle x(i, \tau + 1) - x(i, \tau)\rangle \tag{6}$$

in a world-line quantum Monte Carlo algorithm [62–64] in order to examine interacting disordered bosons on a lattice. In Eq. (6), x is the position of a particle i at the imaginary time τ, and N_b is the number of particles. $j(\tau)$ measures the number of particles moving to the right minus those moving to the left. It should be emphasized that BS used the Fourier transform to get the superfluid fraction since they are working at fixed $W = 0$. Indeed, BS demonstrated the absence of a superfluid fraction in their system, and we do find the same. Within this context, it is worth stating that according to Fisher *et al.* [35], a Bose-glass phase will be present instead of a Mott insulator in a disordered system if (1) the superfluid fraction is zero; (2) the compressibility does not vanish; and (3) there is no gap ($\Delta_g = 0$). It may then be that these three conditions are satisfied by our results here, but whether we have a Bose glass remains to be explored. Although we are referring here to the "fluid" of Refs. [17,18], we are currently not able to access their weakly interacting regime as $\gamma \to 0$, because of computational difficulties, to test the response of σ_J as the system approaches a Mott-like insulator or a Bose glass.

III. APPLICABILITY AND IMPORTANCE OF THE PRESENT WORK

Gornyi *et al.* [55] noted that weak localization is applicable to strongly correlated 1D electron systems such as in disordered quantum wires, i.e., with a concentration of impurities. The impurities in a quantum wire provide obstacles to the motion of electrons in the bulk of its material and play the same role as a speckle potential that reduces the mobility of bosons in 1D. Should disordered quantum wires be analyzed by PI methods, the presently proposed MWPF may arise as a convenient measure that can be related to their conductivity.

This is because σ_J, besides being a MWPF, can also act as a measure for the strength of localization. It can be related to the strength of electron localization in a disordered 1D quantum wire. When the localization of electrons becomes stronger, the conductivity is reduced. A repulsive interaction is said to enhance the disorder-induced localization. Now σ_J declines with increasing γ so that the MWPF can find applicability in the study of the behavior of the conductivity versus γ in a quantum wire with impurities in it. According to Gornyi *et al.* [55], an arbitrarily weak disorder leads to a localization of all electronic states so that the dc conductivity $\sigma(T)$ becomes zero for any T. This is analogous to the superfluid fraction being completely depleted in our systems, albeit because of the presence of strong disorder.

Moreover, these authors stated that much less is known about Luttinger liquids in disorder. In fact, this is related to the present case of the "fluid" whose nature is not quite understood, but our current results shed more light on this and may lead to a further understanding.

It may be possible to take a further approach in the future and evaluate the Kubo conductivity by taking the Fourier transform of the current-current correlator, that is,

$$\int_0^\beta e^{i\Omega\tau} \langle \mathcal{T} J(\tau) J(0) \rangle d\tau, \tag{7}$$

where Ω is an external driving frequency, in which case it will not vanish as in the case of Eqs. (4) and (E6). This will be the subject of a future investigation. Here, we wanted to concentrate on σ_J.

Based on our current results, it may be useful to take the important research of Masella *et al.* [28] already mentioned in the Introduction further and evaluate the compressibility, kinetic energy, and MWPF σ_J as functions of the interaction strength γ and T.

It is worth noting that superfluidity in a 1D disordered bosonic system is analogous to superconductivity in a 1D dirty quantum wire. In addition, the localization of bosons in a speckle potential is analogous to the localization of charge carriers in nanoelectronics because of impurities. Further, the conductivity of a nanowire is proportional to the free electron density n [65]. The correlation (coherence) length ξ is proportional to the density of free electrons n [66], and is therefore proportional to the conductivity of the nanowire. Localization of the electrons suppresses the conductivity [67], whereas an increase in ξ such that it becomes longer than the wire suppresses localization.

IV. METHOD

A. System

The system considered is a 1D fluid of N bosons confined by a random potential. The units applied are given in Appendix A. The interparticle interactions are repulsive and described by the two-particle density matrix in Appendix B. This system is simulated at various temperatures and numbers of particles to reveal its properties.

B. Worm algorithm

Specifically, a WAPIMC code is applied that has been written by Prokof'ev [68] originally for the simulation of a 1D homogeneous Bose gas with repulsive interactions. This WAPIMC program has also been used in one of our earlier publications [34]. The WAPIMC and a 3D version of this code have been described earlier in detail [41], and the 1D version has been modified to include a speckle potential of the form given in Appendix D below. The simulations have been conducted on the excellent computational cluster of the Max Planck Institute for Physics of Complex Systems in Dresden/Germany. In essence, this was a heavy computational project with each simulation taking about two weeks of CPU time.

C. MWPF

The measure of path fluctuations Eq. (2) is evaluated numerically. One begins by defining the discrete version of $\Delta(\tau)$, which is the same as $(R_\ell - R_{\ell-1})$ in the second term on the right of Eq. (15) below. At a certain time-slice ℓ the discrete Δ_ℓ reads

$$\Delta_\ell = \sum_{i=1}^{N} (x_{i,\ell} - x_{i,\ell-1}), \tag{8}$$

$x_{i,\ell}$ being the position of bead i at time slice ℓ along the WAPIMC polymer path in imaginary time. As is known [33,41], each particle is represented by a closed polymer path. N is the number of particles and ℓ is an index that refers to the imaginary time $\tau = \ell\tau_0$, with τ_0 the time step so that $d\tau \to \tau_0$ in Eq. (2) when the integral is converted back to a sum. Hence

$$\sigma_J = \left\langle \sum_{\ell=1}^{M} \Delta_\ell^2 \right\rangle \tag{9}$$

is the numerical version of Eq. (2), where $\langle \cdots \rangle$ indicates from now on an average over all WAPIMC configurations. Note that Eq. (9) is designed intentionally with the square of Δ_ℓ so as not to sum up to zero in the absence of superfluidity. This is unlike $\int_0^\beta \Delta(\tau)d\tau$, which is practically the same as the winding number W,

$$W = \frac{1}{L} \sum_{\ell=1}^{M} \sum_{i=1}^{N} (x_{i,\ell} - x_{i,\ell-1}), \tag{10}$$

which is zero in the current work. Hence

$$\sum_{\ell=1}^{M} \Delta_\ell = LW \tag{11}$$

vanishes in the absence of superfluidity. Equation (11) is obtained by substituting (8) into (10). Hence, σ_J is not quite the same as W (see Appendix E for a further elaboration on this issue).

D. Compressibility

The compressibility $\chi(\mu)$ [69] reads

$$\chi(\mu) = \frac{L}{T} \langle \delta N^2 \rangle, \tag{12}$$

where $\langle \delta N^2 \rangle$ is the WAPIMC average of the particle number fluctuations.

E. Hamiltonian

The many-body Hamiltonian of the present system reads

$$H = \sum_{i=1}^{N} \left[-\frac{\hbar^2}{2m} \frac{\partial^2}{\partial x_i^2} + V(x_i) \right] + \sum_{i<j} V_{\text{int}}(x_i - x_j), \tag{13}$$

where $V(x_i)$ is the speckle potential (see Appendix D), and

$$V_{\text{int}}(x_i - x_j) = g_{1D}\delta(x_i - x_j) \tag{14}$$

is the pair interaction potential. See Appendix B for further details.

F. WAPIMC energy estimators

1. Kinetic energy

The thermodynamic estimator for the average WAPIMC kinetic energy E_K is given by [33] (see Appendix C)

$$E_K = \left\langle \frac{1}{M} \sum_{\ell=1}^{M} \left[\frac{N}{2\tau_0} - \frac{(R_\ell - R_{\ell-1})^2}{4\lambda\tau_0^2} \right] \right\rangle, \qquad (15)$$

where $\lambda = \hbar^2/(2m)$, m being the mass of a boson and $\hbar$ the reduced Planck constant, whereas $R_\ell = \{x_{1,\ell}, x_{2,\ell}, \ldots, x_{N,\ell}\}$ denotes a set of N-particle positions at time slice ℓ, each two consecutive positions being separated by a time τ_0. (In the present units, this becomes $\lambda = 1$.) Note that the second term on the right-hand side implies a sum over all particles i at positions $x_{i,\ell}$, that is,

$$(R_\ell - R_{\ell-1})^2 \equiv \left[\sum_{i=1}^{N} (x_{i,\ell} - x_{i,\ell-1}) \right]^2. \qquad (16)$$

In that sense, σ_J is practically the same as the "spring" term $\sim (R_\ell - R_{\ell-1})^2$.

A number of important points are worth mentioning here. As stated previously, the PI does not have a wave function per se. If one is in the classical regime at high T, then the path in PIMC is straight and narrow. But one knows that, in the quantum description, the higher excited wave-function states are very much involved at high T and those are definitely wider than the ground state. They have a lot of oscillations and modes, which makes their kinetic energy large. What does seem to happen in the PI is that the width of the path fluctuations gets narrower corresponding to the average "zittering" velocity

$$\bar{v}_{\text{zitter}} \sim \sqrt{\sum_{\ell=1}^{M} \frac{(R_\ell - R_{\ell-1})^2}{\tau_0^2}} \qquad (17)$$

getting smaller and the E_K correspondingly increasing by less cancellation with the first term. The zittering velocity is of course not a real velocity, but an amount of displacement per imaginary time step. Hence, more spatial ground covered at low T corresponds to the wider variety of possible paths, a higher $\bar{v}_{\text{zitter}}$, and lower E_K. Of course, the MWPF is inherently connected to E_K.

Furthermore, at $T = 0$ all the energy can be called zero-point energy E_{zp}. So there we would expect that σ_J is then measuring E_{zp}. As one raises T, there is more excited-state thermal energy, and the percentage of the total energy due to the ground state is reduced. It is therefore anticipated that σ_J decreases because the paths have less variation and are straighter and narrower, so the PI velocity is less. Indeed, on applying the classical isomorphism, when the imaginary velocity decreases because the PI fluctuations get smaller, the kinetic energy gets larger because the $\langle N \rangle / (2\tau_0)$ term is not canceled as much. When the spring term gets big, the PI fluctuations are large and so the kinetic energy gets smaller. That way, one can see that the results of σ_J and E_K are correlated with each other since they are based on the same calculation.

2. Interaction energy

The interaction energy between the bosons is implied in the WAPIMC code via the pair density matrix described in Appendix B. Although we do not display E_I in our results, it is nevertheless useful to state that E_I can be inferred from the zero-distance pair correlation function [70]

$$E_I = \frac{E_{\text{int}}}{\langle N \rangle T_d} = \frac{1}{2} g_{1D} n g_2(0), \qquad (18)$$

but in our paper we were only interested in the kinetic energy. g_{1D} is defined in Appendix B.

G. Diffusion

The ITDC D_0 is a measure for the net displacement by which the particles diffuse through a potential during a given time period. Mathematically, it is given by

$$D_0 = \lim_{t \to \infty} \frac{\langle \Delta^2 x(t) \rangle}{2t}, \qquad (19)$$

with

$$\langle \Delta^2 x(t) \rangle = \frac{1}{\langle N \rangle} \left\langle \sum_{i=1}^{N} [x_i(t) - x_i(0)]^2 \right\rangle, \qquad (20)$$

where $x_i(t)$ is the position of particle i at time t. Note that in WAPIMC we replace t by the imaginary time τ and take the limit $\tau \to \beta$ assuming β is large enough. In this regard, D_0 is compared against the MWPF σ_J to determine possible connections.

The reason for replacing real time by imaginary time in our Eq. (19) is to enable a PIMC evaluation of this quantity. Further justification for the latter replacement arises from previous works. For example, Ceperley [33] in his review article also uses imaginary time τ to define a velocity in the kinetic energy estimator E_K [our Eq. (15)] where real time is replaced by imaginary time. Rabani *et al.* [71] presented a method to study the transport properties in highly quantum liquids where they also utilized an imaginary time velocity. In Ref. [71], on p. 1130, the real time t in their Eq. (4), containing the frequency-dependent diffusion constant $D(\omega)$, is replaced by $-i\tau$.

H. Pair correlations

The pair correlations are formally given by the function

$$g_2(x - x') = \frac{\langle \psi^\dagger(x)\psi^\dagger(x')\psi(x')\psi(x) \rangle}{\langle \psi^\dagger(x)\psi(x) \rangle}, \qquad (21)$$

where $\psi(x)$ is the wave function. However, there is no wave function in WAPIMC; rather, g_2 is evaluated by binning the number of pairs of particles being at separations $x - x'$. $g_2(0)$ is then evaluated by extrapolating $g_2(x - x')$ towards $x - x' = 0$.

V. RESULTS

A. Superfluid fraction

The superfluid fraction ρ_s/ρ in all of the present samples has been measured to be zero. ρ_s/ρ is as usual obtained

from [60]

$$\frac{\rho_s}{\rho} = \frac{\langle W^2 \rangle}{2\lambda \beta N},$$

(22)

where $\beta = M\tau_0$, and W is given by (10). Thus there is no need for a further elaboration on this quantity.

B. Effect of γ

Although the real physical meaning of changing γ arises if one chiefly varies a_{sc} in Eq. (B3), and not only $\langle N \rangle$ as in the present work, we are nevertheless driven by curiosity to explore what happens when properties are graphed against γ instead of the legitimate $\langle N \rangle$ [or density $n = \langle N \rangle / L$ in γ]. The $\langle N \rangle$ is also an important property of the system since all types of energies, i.e., kinetic, potential, and interactions, stand in direct proportionality to $\langle N \rangle$. We therefore assume a γ that is varied artificially and solely via $\langle N \rangle$ through the chemical potential μ. Herein, the role of $\langle N \rangle$ is explored in defining the behavior of σ_J, D_0, $\chi(\mu)$, E_K, and $g_2(0)$. In Figs. 1–4, the latter properties are plotted against γ at various T. Three different speckle strengths $\langle V \rangle$ and two scattering lengths a_{sc} are considered.

1. σ_J and D_0

In Fig. 1(a), σ_J [Eq. (9)] declines with γ because an increase in repulsive interactions makes it harder for bosons to spread through the speckle potential, thus increasing their localization. This decreases their zitter motion and the imaginary velocity Eq. (17). That is somewhat equivalent to having a narrower, i.e., more nearly classical path so σ_J decreases. So, perhaps the decrease in σ_J and the width of the wave function could hang together.

We were not able to approach the weakly interacting regime, let alone $\gamma = 0$, by increasing $\langle N \rangle$ to very large values because of computational and technical challenges. The PI fluctuations spread more through the speckle at a lower γ (larger particle density n) because the probability for bosons to tunnel through the random potential becomes higher. This is a rather surprising result, a manifestation of the inverted role the Lieb-Liniger parameter can play in such a setup.

At a fixed value like 0.5 on the γ-axis of the graphs, a higher T reduces σ_J and with it its rate of decline with γ. The reduction of σ_J with T arises because in Eq. (15), the spring term $\sim (R_\ell - R_{\ell-1})^2$ shrinks with increasing T instead of expanding according to the classical isomorphism [33]. It is thus argued that the "spring constant"

$$\frac{1}{4M\lambda\tau_0} \to \frac{k_B T}{4\lambda}$$

(23)

increases with T. The fluctuations shrink because the exponential weight factor would involve the high "kinetic energy" $\propto (dx/d\tau)^2$ over a shorter total imaginary time β.

The ITDC D_0, on the other hand, is less sensitive to changes in γ than σ_J and is therefore not a good indicator for variations in the MWPF in a speckle potential. In contradiction to σ_J, D_0 is generally larger for higher T at all γ and does not obey the classical isomorphism.

In Fig. 1(b), for a lower $\langle V \rangle$ and a_{sc}, the behavior of σ_J and D_0 is qualitatively the same as in (a) at the same T
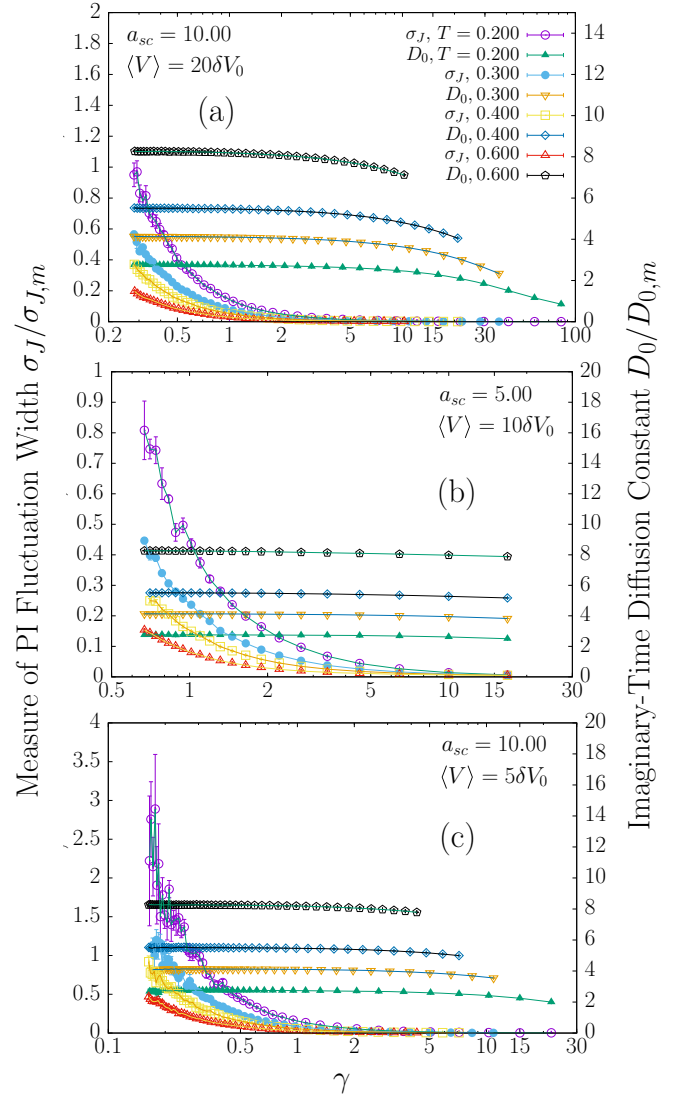

FIG. 1. Left y-axis: measure of the width of path integral fluctuations σ_J [Eq. (9)] as a function of the Lieb-Liniger interaction parameter γ. $\sigma_{J,m} = 60$ and $D_{0,m} = 30$ are reference values. Right y-axis: ITDC D_0 [Eq. (19)] vs γ. Plots are at various temperatures T, speckle strengths $\langle V \rangle$, and two different scattering lengths a_{sc}. Legends are the same in all frames. Frame (a) is for $\langle V \rangle = 20\delta V_0$ and $a_{sc} = 10$. Frame (b) is as in (a), but for $\langle V \rangle = 10\delta V_0$ and $a_{sc} = 5.00$, and (c) for $\langle V \rangle = 5\delta V_0$ and $a_{sc} = 10$. σ_J and a_{sc} are in units of ℓ_c^2 and ℓ_c, respectively; $\mathcal{D}_0$, $\langle V \rangle$, and T are in units of T_d, whereas γ is unitless.

values. Upon a quantitative comparison of (b) to (a), there are no significant differences in their rates of change with γ, although D_0 in (b) is more robust to variations in γ than in (a).

In Fig. 1(c) at an even lower $\langle V \rangle$, but the same a_{sc} as in (A), σ_J and D_0 display the same qualitative behavior as in either (a) or (b). There is an interplay between $\langle V \rangle$ and a_{sc} in defining the magnitudes of σ_J and D_0. It is further anticipated that changing γ by $\langle N \rangle$ has different outcomes from changing it by a_{sc}.
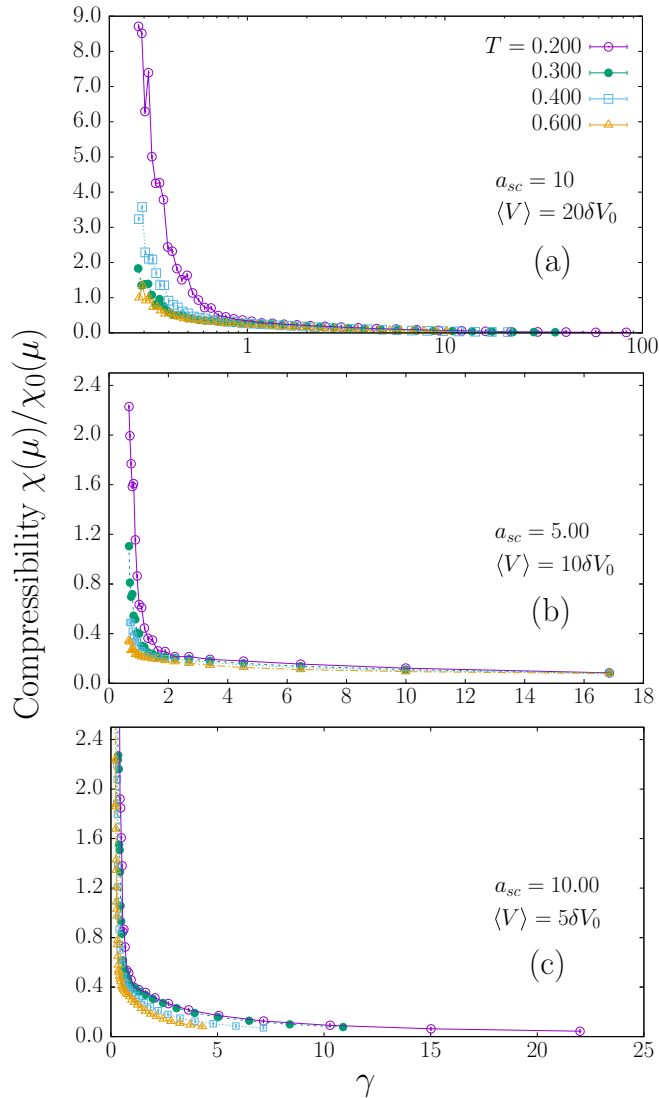
FIG. 2. As in Fig. 1, but for the WAPIMC compressibility $\chi(\mu)$ [Eq. (12)]. $\chi(\mu)$, $\langle V \rangle$, and T are in units of T_d, whereas a_{sc} is in ℓ_c and γ is unitless. The normalization factor is $\chi_0(\mu) = 10^5$.

2. Compressibility $\chi(\mu)$

In Fig. 2(a), $\chi(\mu)$ [Eq. (12)] rises steeply as γ approaches zero and drops significantly towards zero at the larger γ. This occurs in all frames with different pairs of a_{sc} and $\langle V \rangle$, from which one concludes that the interplay between a_{sc} and $\langle V \rangle$ has practically no influence on the qualitative behavior of $\chi(\mu)$. The presence of a diverging $\chi(\mu)$ at $\gamma \to 0$ and a finite $\chi(\mu)$ at the larger γ signals the presence of two nonsuperfluid phases, a fluid and a possible Bose-glass phase, respectively. It has been noted earlier in Sec. III that the conductivity of a nanowire is proportional to the free-electron density. Since a system of bosons in disorder is analogous to a dirty quantum wire, the role of bosons in the conductivity is analogous to that of electrons, given that bosons in 1D behave like spinless fermions. Therefore, in the case of a larger number of bosons and a lower γ, our system becomes more "conducting." As such, when $\gamma \to 0$ our system becomes a conducting bosonic fluid.

$\chi(\mu)$ mostly declines with T at the lower γ. Thus a further rise in T could eventually cause $\chi(\mu)$ to approach zero towards an insulating state. Indeed, a possible transition at finite temperature is between two non-SF phases in the *global* sense. But in the *local* sense, it is possible to have a Bose-glass phase [9,25]. In addition, an Anderson glass may exist as well [25].

A Bose-glass at finite T in 1D disorder has been characterized by Gori *et al.* [19] via the inverse correlation length in their Fig. 12. It has been shown that the thermal correlation lengths are much larger than the localization lengths so that the quantum nature of the Bose-glass phase is preserved up to a crossover temperature. Further, the strongly correlated phases predicted at $T = 0$ K persist at finite T of their experiment.

Since we are dealing with an anomalous and unusual *fluid*, we therefore propose the existence of a Bose-glass phase. This can be inferred from the behavior of the compressibility $\chi(\mu)$ in Fig. 2 of our paper, which demonstrates a transition at a critical γ. Given the fact that the fluid is unusual, we could argue that it is quite justified to make assumptions.

Svistunov *et al.* [69] explained the 1D Bose-glass phase at finite temperature as localized condensates well separated from each other with a superfluid density that is predicted to be exponentially small for large separations between the lakes. Moreover, it is important to distinguish between *global* and *local* superfluidity (SF). Thus, while there may be no global SF, the disorder potential could host localized isolated SF lakes in the way Vosk and Altman [8] showed. Hence, there is a difference between local SF which cannot be detected with a PIMC winding number calculation and the global SF which can. The concept of global and local SF has been addressed in an optical lattice in one of our earlier publications [72].

3. Kinetic energy E_K

Figure 3(a) illustrates the kinetic energy E_K [Eq. (15)] as a function of γ for various $\langle V \rangle$ and at different T. E_K displays stronger localization of the bosons as it rises steeply at the lower $\gamma \overset{<}{\sim} 2$ beyond which it kinks over tending towards a plateaulike behavior. The latter is mostly pronounced at $T = 0.2$ and 0.3, and it indicates that the localization strength stabilizes at the larger γ. The rise towards a plateau occurs because the spring term in Eq. (15) becomes smaller as the wave function shrinks with γ causing lesser cancellation of $\langle N \rangle / (2\tau_0)$. The curve of E_K versus γ shifts upward to higher values at larger T indicating that the spring term shrinks further with T towards stronger localization. In (b), the behavior of E_K is surprisingly different from that in (a). For a weaker $\langle V \rangle$ and a_{sc}, and as T is increased, E_K versus γ tips over from an initially steeply declining to an increasing behavior at the lower γ. Nevertheless, E_K assumes higher values at the larger T as in (a). The tipover in the behavior of E_K can obviously be ascribed to the change in the behavior of the spring term because of the lower $\langle V \rangle$ and not a_{sc}. This is because in frame (c), for an even lower $\langle V \rangle$ but the same a_{sc} as in (a), this tipover is also observed upon a closer inspection. Hence, a_{sc} is ineffective in inducing the tipover. In (c), E_K has again larger values at higher T. What is also worth noting is that the curves in all frames tend to converge to the same point as $\gamma \to 0$.
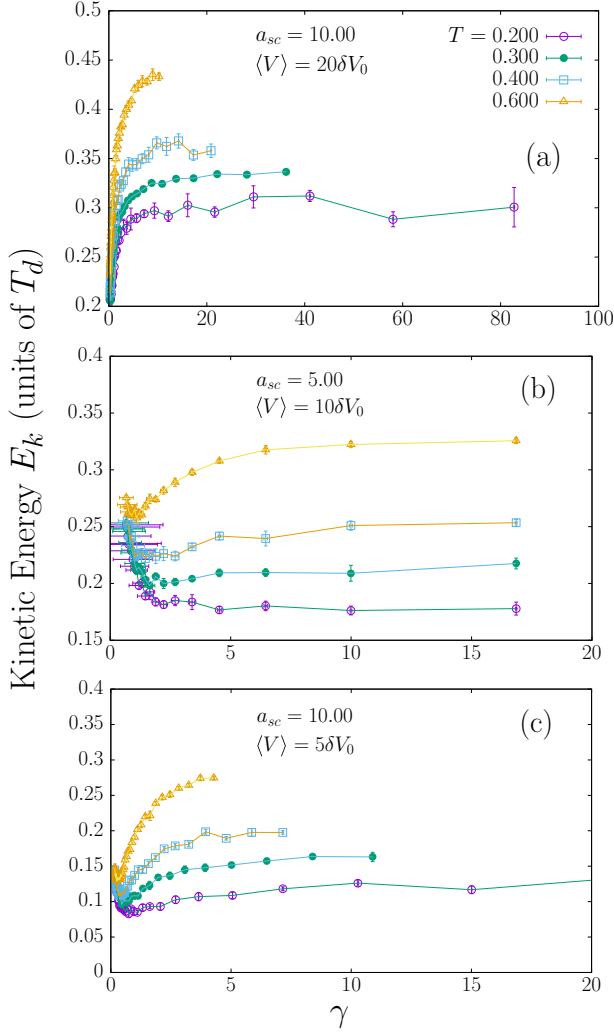
FIG. 3. As in Fig. 1, but for the WAPIMC kinetic energy E_K [Eq. (15)]. E_K, $\langle V \rangle$, and T are in units of T_d, whereas a_{sc} is in ℓ_c and γ is unitless.

Whether this may be the key to observing a reentrant fluid-insulator transition in future WAPIMC simulations remains to be seen.

The increase of E_K with γ can be understood based on an argument formulated from Ref. [69]. Consider particles localized in potential minima arising from their mutual repulsion. If the repulsive energy is U that is proportional to the δ-function interaction, then quantum mechanics will give the particles a delocalization,

$$\eta \sim \sqrt{\hbar}/(U'')^{1/4}, \qquad (24)$$

where $U'' \sim \gamma$, U'' being the second derivative of $U(r)$ with respect to the interparticle distance r. Since the zero-point kinetic energy is determined by η such that

$$E_K \sim \frac{\hbar^2}{2m\eta^2}, \qquad (25)$$

then from (24) one has that
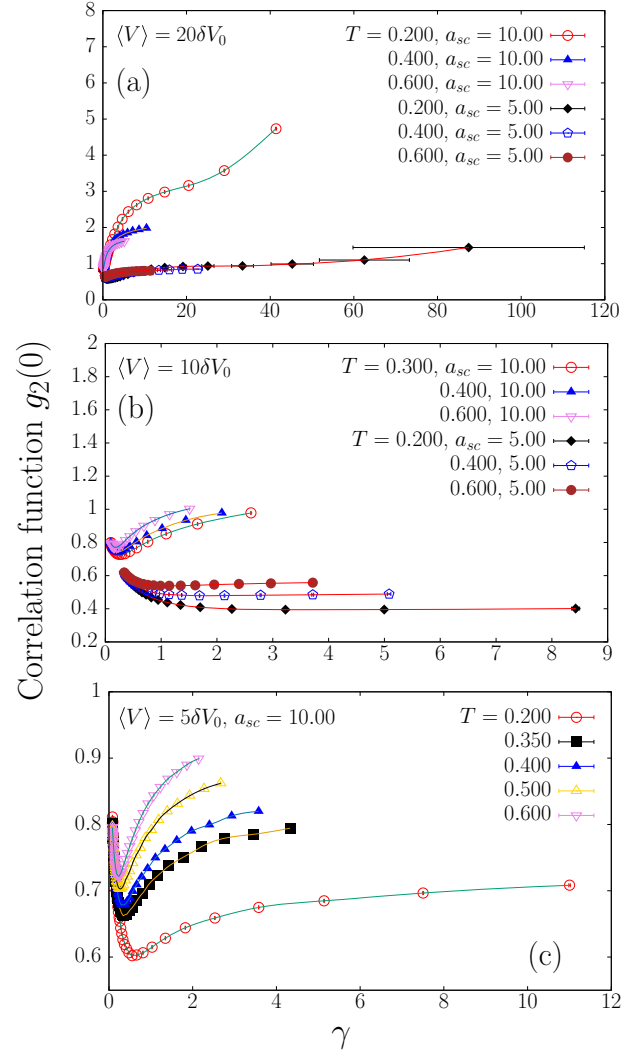
$$E_K \sim \sqrt{U''} \sim \sqrt{\gamma}, \qquad (26)$$

FIG. 4. Second-order correlation function $g_2(0)$ as a function of the interaction parameter γ at various temperatures T, three speckle strengths $\langle V \rangle$, and two scattering lengths a_{sc}. Frame (a) is for $\langle V \rangle = 20\delta V_0$; (b) is as in (a), except for $\langle V \rangle = 10\delta V_0$. Frame (c) is as in (a), but for $\langle V \rangle = 5\delta V_0$. a_{sc} is in units of ℓ_c, $\langle V \rangle$, and T in T_d, and γ is unitless.

and $\eta \sim 1/\gamma^{1/4}$ so that delocalization because of zero-point motion declines with γ, except for certain values of $\langle V \rangle$ like $10\delta V_0$, where the tipover is recorded. Consequently, σ_J is proportional to the extent of delocalization η and declines with γ. This is a behavior that seems anomalous because according to Refs. [17] and [18] one would have expected that a decreasing γ towards zero would lead from a fluid to an insulator rather than in the direction it seems to be going. However, one must not forget the presence of the speckle potential that screens part of the interactions and captures particles in its local minima as well. Indeed, interactions and speckle-strength play a decisive role in localization processes.

Upon a comparison of Fig. 3 with 1, it can be seen that E_K displays generally a largely different response from σ_J to changes in γ. However, E_K and σ_J are really the same thing and the different response is just a matter of scale since we have $E_K = c_1 - c_2\sigma_J$, where the c_i are constants. When σ_J

goes up, E_K has to go down if the first term $c_1 \propto \langle N \rangle$ does not change, but the relative response is determined by just the c_i. Moreover, E_K is not exactly the "opposite" of σ_J because $\langle N \rangle$ in the first term c_1 depends on γ. This dependence contributes to the complexity in the behavior of E_K displayed in Fig. 3.

From Figs. 1(a) and 3(a) at $\langle V \rangle = 20\delta V_0$, it can be deduced that σ_J declines with increasing zero-point kinetic energy E_K due to a decrease in η where $E_K \sim (\hbar/\eta)^2$. In a crystal lattice, for example, particles can get localized in the minima of the potential wells. As such, they undergo local oscillations with a delocalization η that governs E_K. The same occurs in the minima of the speckle potential. It turns out then that E_K is proportional to the extent of localization. This is because according to Eq. (15), the second term on the right-hand side, which is the same as σ_J, is subtracted from $N/(2\tau_0)$. Consequently, σ_J is connected to the zero-point motion implied by E_K via η [8].

Further understanding of the behavior of σ_J versus η can be reached by referring to the momentum-position uncertainty principle $\Delta p \Delta x \sim \hbar$. In that sense, $\eta \sim \Delta x$ and $E_K \propto (\Delta p)^2$, and therefore when the wave functions of the particles spread out more, Δp drops and so does E_K, whereas σ_J rises. As such, our σ_J can thus be viewed as a measure for the width of the many-body wave function in the current speckle potential.

4. $g_2(0)$

Figure 4 displays the pair correlation function $g_2(0)$ (see Sec. IV H) as a function of γ. In frame (a), $g_2(0)$ for $a_{sc} = 10$ shows an initial steep rise at the lower γ and then it kinks over. At a value like ~ 5 along the γ-axis, the curve $g_2(0)$ shifts slightly downward for higher T. On the other hand, for $a_{sc} = 5.00$ its dependence on T and γ is much weaker than for $a_{sc} = 10$ and almost linear, manifesting the striking reality that a_{sc} controls also the response of $g_2(0)$ to T and γ. The behavior of $g_2(0)$ for $a_{sc} = 10$ can be related to E_K in Fig. 3(a). The initial steep rise of $g_2(0)$ at the lower γ corresponds to that of E_K. In Fig. 4(b) for a lower $\langle V \rangle$, $g_2(0)$ for $a_{sc} = 10$ drops initially with γ until it reaches a minimum beyond which it rises again, perhaps tending towards a plateau. For $a_{sc} = 5.00$, $g_2(0)$ just drops with γ towards a plateau. This is in correspondence to the behavior of E_K in Fig. 3(b) at $T < 0.600$, where the localization strength initially drops at the lower γ and then heads towards a plateau at the larger γ. It only makes sense that a decrease in the localization causes $g_2(0)$ to decline in this case as the wave function expands and the distance between the particles increases, thus lowering the correlation length. In Figs. 4(b) and 4(c), the curve of $g_2(0)$ shifts upward for higher T in contrast to (a). That is to say, the strength of the speckle potential controls the response of $g_2(0)$ to T. In Fig. 4(c), for an even lower $\langle V \rangle$, the minimum observed in (b) for $a_{sc} = 10$ occurs here also in a more pronounced fashion, and a similar behavior is displayed for $g_2(0)$ as in (b). One can contrast the latter result with E_K in Fig. 3(c) as there is a correspondingly similar dependence on γ with a minimum. One could ascribe to this feature a most likely fluid-insulator phase transition.

C. Effect of temperature

Figure 5 displays the same properties of the fluid as in the previous section, but now as functions of T. The goal is to look
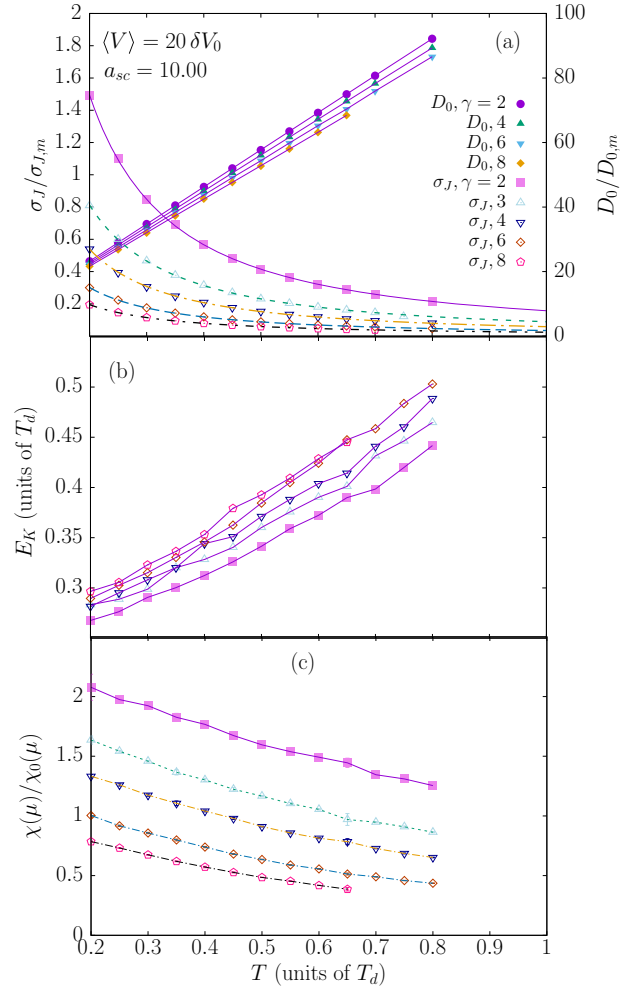

FIG. 5. Measure of the width of path integral fluctuations (MWPF) σ_J [Eq. (9)], ITDC D_0 [Eq. (19)], and kinetic energy E_K [Eq. (15)] as functions of temperature T and at various values of γ. The strength of the speckle potential is $\langle V \rangle = 20\delta V_0$ and the scattering length is $a_{sc} = 10$. Frame (a) displays σ_J (left axis) and D_0 (right axis), where $\sigma_{J,m} = 2.0$ and $D_{0,m} = 3.5$ are reference values. Frame (b) displays E_K at γ with the same values and legends as in (a) for σ_J. Frame (c) is as in (b), but for $\chi(\mu)$, which is normalized by $\chi_0(\mu) = 10^5$. D_0, E_K, μ, T, and $\langle V \rangle$ are in units of T_d, a_{sc} in ℓ_c, and σ_J in ℓ_c^2.

at them again from another angle, although the T-dependence has already been manifested indirectly in Figs. 1–3.

1. σ_J and D_0

Figure 5(a) demonstrates that σ_J declines exponentially with increasing T. Furthermore, the whole curve of σ_J shifts downward for larger γ, which corresponds to what is observed in Fig. 1. Nevertheless, the goal here is to clearly reveal the temperature dependence. On the other hand, the ITDC D_0 rises linearly with T, which is dramatically different from the behavior of σ_J. The slope of D_0 versus T declines with γ because the repulsive interaction constitutes a potential barrier between the 1D bosons which they have to overcome in order to travel from one end of the system to the other. At higher repulsion, more energy is thus required to surmount

the barrier in order to diffuse to longer distances, therefore reducing D_0. With increasing T further beyond the displayed range, it is anticipated that eventually $\sigma_J \to 0$ showing that MWPF becomes quite small, therefore raising the uncertainty in the momentum of the particles. Once again, the behavior of σ_J with T is in line with the classical isomorphism, namely that the MWPF of the bosons decreases with T instead of increasing with it.

2. Inapplicability of Luttinger's liquid theory

The calculations of the winding number W reveal that the superfluid is completely depleted in the present system, which is a manifestation of the strength of the disorder used and which is in line with the findings of Ref. [61]. Further, condensation in the speckle potential exists only at low values of $\langle V \rangle$ [73] and therefore it is unlikely that the present system harbors any condensate that could be connected to a superfluid. Since the superfluid fraction n_s is absent in all of the present samples, the superfluid stiffness given by [69]

$$\Lambda_s = n_s \langle N \rangle / m = LT \langle W^2 \rangle \qquad (27)$$

is zero, where W is the winding number [33]. Therefore, the Luttinger parameter $\bar{K} = \sqrt{\chi \Lambda_s}$ is also zero, where χ is the compressibility. This suggests that the current strongly disordered system cannot be described by Luttinger's liquid theory.

3. Zero-point kinetic energy E_K

In frame (b) of Fig. 5, E_K rises almost linearly with T for all values of γ displayed. This demonstrates the rather interesting result that the first term on the right-hand side of (15), being the classical kinetic energy, overwhelms the second term arising from the path integral. That is, E_K seems to be largely classical and dominated by $\langle N \rangle$, although the above two terms compete with each other. All that is happening is that the increase in kinetic energy is due to simple thermal excitations in the states, that certainly would lead to a diminishing of σ_J without any insulator nature being involved. Indeed, the increase in D_0 would make sense then.

4. Compressibility χ

In frame (c) of Fig. 5, $\chi(\mu)$ declines almost linearly with T. It further shifts to lower values at higher γ for all T. These results demonstrate again the approach towards an insulating state as the system becomes less compressible. The latter supports σ_J decreasing and E_K rising with T.

D. Role of chemical potential

Figure 6 displays σ_J, D_0, and E_K as functions of μ at fixed T. In frame (a), at $\langle V \rangle = 0$ and $5\delta V_0$, σ_J rises steadily with μ displaying some fluctuations at the higher μ, which arise most likely because of uncertainties in the WAPIMC number of particles $\sqrt{\langle \delta N^2 \rangle}$, where $\langle \delta N^2 \rangle = \langle N^2 \rangle - \langle N \rangle^2$. For $\langle V \rangle = 20\delta V_0$, σ_J rises initially only slowly with μ up to $\mu \sim 1.8$, beyond which it begins to increase faster. This shows that as $\langle V \rangle$ is increased, a larger number of particles is required to overcome the potential barriers of the speckle potential in order for the MWPF of the bosons to rise.
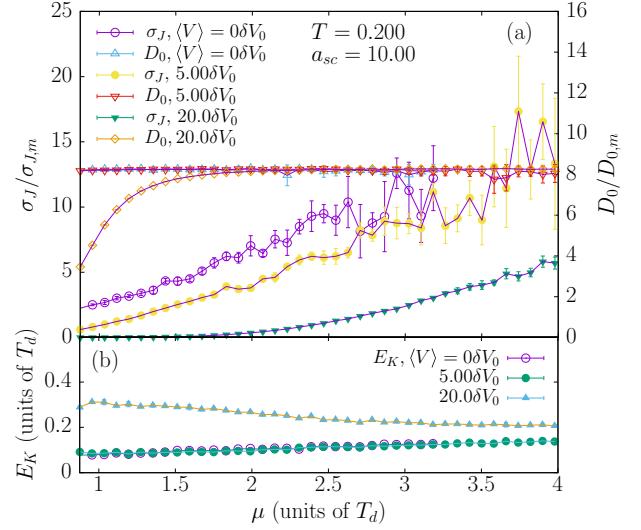

FIG. 6. Same properties as in Fig. 5, but as functions of μ and a few different values of $\langle V \rangle$. The temperature is $T = 0.200$ and the scattering length is $a_{sc} = 10$. Frame (a) shows σ_J (left axis) and D_0 (right axis), where $\sigma_{J,m} = 10$ and $D_{0,m} = 10$ are reference values. D_0, E_K, μ, and T are in units of T_d, a_{sc} in ℓ_c, and σ_J in ℓ_c^2.

When $\mu \lesssim \langle V \rangle$ is still large enough to "cover" the speckle, the particles occupying it form what is called disconnected lakes [8,18,69], where each lake has a size r_ℓ determined by μ. Let us assume that the present system harbors no local superfluid but rather patches or lakes that are composed of a normal fluid. An increase in μ, then, yields a rise in r_ℓ upon which the energy gap between successive speckle-potential energy-levels i [69],

$$\delta E = E_{N_i+1} - E_{N_i} \sim g_{1D}/r_\ell, \qquad (28)$$

is reduced, where N_i is the occupancy of level i, and g_{1D} is given by Eq. (B2). Therefore, less energy is required to excite particles to higher-energy states that contribute to σ_J when the lakes become larger. In the systems presented here then, when $r_\ell \ll d_\ell$, where d_ℓ is the separation between two lakes, a global *fluidity* is absent. The distance between two lakes d_ℓ is reduced when r_ℓ is increased so that the tunneling amplitude between them, given by $\Gamma \propto \exp(-d_\ell/r_\ell)$, goes up. A rise of σ_J with μ implies, therefore, that $\sigma_J \propto r_\ell$. The latter arguments explain further why σ_J declines with γ in Fig. 1. Since $\gamma = 2/(n a_{sc})$, it is also $\sim 1/\mu$ and therefore a higher γ results from a lower $\mu \sim r_\ell$ yielding a lower Γ. Hence, Γ drops with increasing γ reducing therefore σ_J. When μ is reduced to an extent that Γ becomes very small, particle exchange between the lakes is blocked by interactions. A rise in $\langle V \rangle$ reduces σ_J obviously for all μ at fixed a_{sc}. This is also because the size of the lakes r_ℓ for a given μ declines with rising $\langle V \rangle$ causing a reduction in the tunneling amplitude Γ. At higher $\langle V \rangle$ then, the interplay between interactions and disorder causes a stronger localization of the particles than at lower $\langle V \rangle$.

On the other hand, the ITDC D_0 shows again different features. For $\langle V \rangle = 20\delta V_0$ it rises with μ until at $\mu \approx 1.6$, which is largely determined by the strength of the speckle potential, D_0 saturates at the same plateau value as for the

rest of $\langle V \rangle$. As such, it conveys no further important information about the fluid. Note that D_0 shows variations with μ only for $\langle V \rangle = 20\delta V_0$ while for $\langle V \rangle = 0$ and $5\delta V_0$ it is much less sensitive to changes in μ given that D_0 remains practically constant. Hence, one concludes that D_0 does not see the speckle potential when $\mu > \langle V \rangle$ and particularly for low values of $\langle V \rangle$ approaching zero.

In Fig. 6(b) for $\langle V \rangle = 20\delta V_0$, E_K declines with increasing μ suggesting that the second term on the right-hand side of Eq. (15) is changing at a higher rate than the first term thus overcoming the classical effects arising from $\langle N \rangle/(2\tau_0)$. The drop of E_K with rising μ—that is also with $\langle N \rangle$—is because a larger number of repulsively interacting particles increases the rate of boson-boson scattering, a process that serves to "kick" the particles out of their confinement in the speckle potential into the conduction band. As a result, the number of localized particles is reduced, and with it E_K.

In the absence of a speckle potential ($\langle V \rangle = 0$) and when $\langle V \rangle = 5\delta V_0$, E_K rises linearly with μ implying that $E_K \propto \langle N \rangle$. Thus there seems to be a critical value for $\langle V \rangle$ at which an inversion occurs in the behavior of E_K versus μ. This result bears connections to the behavior of E_K versus γ in Fig. 3 that changes with $\langle V \rangle$. Back to Fig. 6 here, a similar argument can be made about D_0 that shows a strong dependence on μ only when $\langle V \rangle = 20\delta V_0$, whereas almost none at lower $\langle V \rangle$.

The response of E_K to changes in μ is therefore governed largely by the magnitude of $\langle V \rangle$ in Fig. 6(b), taking into consideration the previously mentioned competition between the classical and quantum terms of Eq. (15). In any case, one can understand this behavior as arising from the interplay between disorder and interactions. It seems that below a critical $\langle V \rangle$, this interplay is such that a rise in the interactions causes weaker localization of the bosons in the speckle potential minima. At the critical $\langle V \rangle$ and perhaps above, the opposite occurs as the heightened speckle potential screens the interactions and increases the strength of localization. That is, in the former case the interactions override the effects of the speckle, whereas in the latter the contrary occurs. Thus, there is a competition between both effects.

VI. CONCLUSIONS AND FUTURE OUTLOOK

In summary then, the properties of one-dimensional (1D) disordered bosons have been explored in the absence of superfluidity at finite temperature using the state-of-the-art worm algorithm path integral Monte Carlo (WAPIMC) method in the grand-canonical ensemble [41]. The properties of the fluid mentioned in the works of Aleiner *et al.* [18] and Michal *et al.* [17] have been particularly addressed shedding more light on it. One of the problems that we have tackled was to find an order parameter that would describe the measure of the width of path integral (PI) fluctuations (MWPF) in this fluid. In this regard, we proposed a quantity of the form $\sigma_J = (1/\tau_0)\langle \int_0^\beta \Delta^2(\tau)d\tau \rangle$, which is practically the same as the spring term in the kinetic energy estimator of WAPIMC.

Within these contexts, the role of the particle number density n in defining the properties of a 1D disordered repulsively interacting Bose fluid at finite temperature has been explored. The scattering length a_{sc} was kept constant while the number of particles $\langle N \rangle$ was allowed to change in order to artificially

vary the Lieb-Liniger interaction parameter γ. The properties examined were the MWPF σ_J, the ITDC D_0, compressibility $\chi(\mu)$, zero-point kinetic energy E_K, and the pair-correlation function $g_2(0)$. They were explored as functions of γ and the temperature T. The role of the chemical potential μ, and its connection to a possible presence of "lakes" in the speckle, has also been addressed.

The important results of this work accompanied by our comments follow. (i) $\chi(\mu)$ reveals two nonsuperfluid phases, a fluid at $\gamma \to 0$ and a possible Bose glass phase at the larger γ. (ii) E_K varies with γ and μ in astonishingly different ways for different $\langle V \rangle$. The reason might be because a_{sc} has been kept constant and μ varied to increase $\langle N \rangle$ that lowers γ. E_K has particularly been found to signal a transition (perhaps a fluid insulator) by its convergence towards a common value when measured as a function of γ at various T. (iii) If one increases $\langle N \rangle$ the MWPF rises as the bosons become less repulsive and gain more mobility. (iv) We have been able to demonstrate again that an insulator can be obtained by heating. (v) Luttinger's liquid theory cannot be applied to describe 1D bosons in strong disorder at finite T approaching the degeneracy temperature T_d because of the absence of superfluidity that yields a zero Luttinger parameter. (vi) We have been able to show that the strength of the speckle potential $\langle V \rangle$ largely controls the behavior of $\chi(\mu)$, $g_2(0)$, and E_K. (vii) It seems that D_0 does not obey the classical isomorphism as it rises with T; in fact, this is a significant feature that has been manifested by WAPIMC arising as one of the consequences of the interplay between disorder and interactions. In conjunction with finding (ii), it is useful to state that whereas Aleiner *et al.* [18] noted that at the fluid-insulator transition the thermodynamic functions such as the specific heat do not show a singularity, the WAPIMC E_K may be able to detect this transition. The peculiar inversion in the behavior of E_K versus μ as one goes from small to larger $\langle V \rangle$ is a manifestation for a complex influence of the disorder. The tipover of E_K versus γ from an increasing to a decreasing behavior at the lower γ could further signal the above-mentioned transition.

In the future, it would therefore be useful to check if this also holds for the WAPIMC estimators of other properties than the ones studied here. Indeed, the thermodynamics of the fluid-insulator transition are not known, and it has been noted that many-body localization of interacting particles signals a breakdown of conventional thermodynamics [21].

We anticipated that σ_J would display a signal for the two-fluid insulator transition, but unfortunately it has been found that σ_J will only keep rising as γ is lowered. Therefore, there was no signal for a second reentrant transition. In fact, if one wanted to achieve $\gamma \to 0$ by keeping a_{sc} fixed, this sets forth a computational challenge since in order to achieve $\gamma \to 0$ this requires an extremely large number of particles and therefore very long CPU times. Thus, a_{sc} must be allowed to change instead of $\langle N \rangle$ in order to achieve the above-stated purpose of reaching $\gamma \to 0$ without difficulties.

In Sec. III, it has been noted that the conductivity of a quantum wire is proportional to the density of free electrons. In fact, MWPF σ_J takes account of this conductivity if applied to dirty quantum wires. This can be inferred from Fig. 1, where σ_J rises significantly as $\gamma \to 0$ with the rise of boson density that can be set analogous to a rise in the electron density.

This analogy signals that the conductivity of bosons rises as localization is suppressed. Since bosons in 1D behave like spinless fermions, it is very much likely that the coherence length in our system becomes larger than its size as $\gamma \to 0$, much as in quantum wires with electronic currents [67].

In the future, we will explore the present system by changing a_{sc} to explore the fluid-insulator phase transition [17,18]. Then one can set a_{sc} very large so that γ may approach zero. A question of interest to answer is whether a change of γ by a_{sc} while keeping n fixed would yield the same results as changing it in the opposite way. It would also be interesting to examine σ_J, e.g., as a function of the length of the system, or the energy along the lines of Ref. [74]. One could also address other questions related to the presence of any special features in the Matsubara Green's function. Do we have particles or holes, and how does their weight change with γ and T? Moreover, in case one is able to prove the presence of local superfluid lakes in the absence of a global superfluid, would it then make sense to apply Luttinger's liquid theory to these lakes locally?

APPENDIX A: UNITS AND PARAMETERS

The temperature and energy are given in units of the degeneracy temperature T_d, where $T_d = 2\pi\hbar^2 n_0^2/m$. In the WAPIMC code, $m = 0.5$, $k_B = 1$, and $\hbar = 1$ and hence $T_d = 4\pi n_0^2$. It should be emphasized that T_d is computed from an initial density parameter n_0 that is only used to fix the size of the system and to initialize the number of particles in the WAPIMC simulation. That is, n_0 is not updated during the simulations, and the final density of the system n is usually different from the initial n_0. In the current simulations, n_0 is unitless and is set to 1. Lengths are in units of ℓ_c, the correlation length of the speckle potential, and the system size is $L/\ell_c = 1000$. Moreover, the boundary conditions are periodic so as to enable a computation of the WAPIMC winding number.

The speckle potential was generated to be in arbitrary units (see Appendix D) with a strength of $\Delta_0 = 1.33322$. There is nothing special about this number, since it can be magnified or reduced via a multiplication factor. Assuming $\Delta_0 = \delta V_0 T_d$, i.e., a number δV_0 multiplied by the unit T_d, then $\delta V_0 = \Delta_0/T_d = 0.10609$ is in units of T_d. δV_0 is the unit by which we define $\langle V \rangle$.
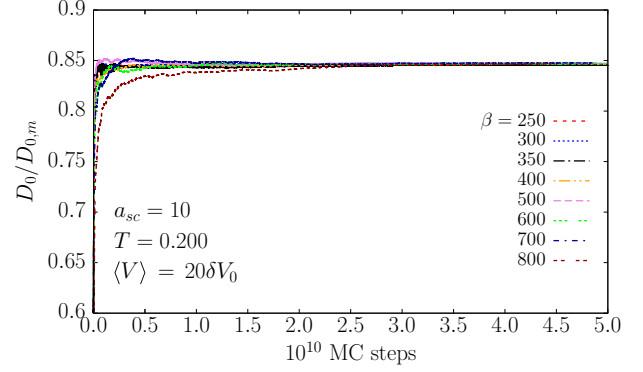

FIG. 7. WAPIMC ITDC D_0 [Eq. (19)] as a function of the simulation time (MC steps) for several values of $\beta = M\tau_0$. $D_{0,m} = 30$ is the same reference value as in Fig. 1. The sample is at the parameters $T = 0.200$, $a_{sc} = 10.0$, and $\langle V \rangle = 20\delta V_0$. T and $\langle V \rangle$ are in units of T_d, whereas a_{sc} is in units of ℓ_c.

The time step of the simulation $\tau_0 = 1/(MT)$ was kept constant at 2.5×10^{-3} while M was varied to change T. The range of μ considered is from $10/T_d$ to $50/T_d$, whereas T changes from 0.200 to 0.600. The simulations where conducted for each μ and T, and it took about 14 days of CPU time for each sample to reach thermalization.

In our simulations, $\beta = M\tau_0 = 400$ is considered large enough for the validity of Eq. (19). To prove this, we conducted simulations with β ranging from 250 to 800 to demonstrate that all of them converge at the same value of the ITDC. Figure 7 displays this feature for $D_0/D_{0,m}$ as a function of simulation time, or Monte Carlo steps. Even $\beta = 250$ seems to be large enough for our purposes.

APPENDIX B: INTERACTIONS

The interactions between the bosons in 1D are accounted for by the exact two-particle density matrix given by (see, e.g., Ref. [75])

$$\rho(x_{ij,\ell}, x_{ij,\ell-1})$$

$$= 1 - \sqrt{\frac{\hbar^2\tau_0}{4ma_{sc}^2}} \exp\left\{ \frac{m}{4\hbar^2\tau_0}(x_{ij,\ell} - x_{ij,\ell-1})^2 \right.$$

$$\left. + \frac{|x_{ij,\ell}| + |x_{ij,\ell-1}|}{a_{sc}} + \frac{\hbar^2\tau_0}{ma_{sc}^2} \right\}$$

$$\times \mathrm{Erf}\left[\sqrt{\frac{\hbar^2\tau_0}{ma_{sc}^2}} + \left(\frac{|x_{ij,\ell}| + |x_{ij,\ell-1}|}{a_{sc}} \right)\sqrt{\frac{ma_{sc}^2}{4\hbar^2\tau_0}} \right],$$

$$\tag{B1}$$

where as before $\hbar = k_B = 1$, $m = 0.5$, $\tau_0 = \beta/M$ is the imaginary "time step" with $\beta = 1/T$ the inverse temperature, T being in units of the degeneracy temperature T_d, $(x_{ij,\ell}, x_{ij,\ell-1})$ the relative positions of two particles i and j along the x-axis at two different time slices ℓ and $\ell - 1$, respectively, a_{sc} is the 1D scattering length, and m is the mass of a boson. Equation (B1) appears in the worm-update probabilities of the WAPIMC code as a multiplicative factor. It should, however,

be noted that *technically speaking* the exponential in Eq. (B1) is multiplied by a correction term of the form of an error function.

Thus many-body interactions are taken into account by a product of several terms $\rho(x_{ij,\ell}, x_{ij,\ell-1})$ with each other for pairs of particles i and j. The resulting chain of ρ terms takes care of the many-body effects. The interactions are in other words effectively described by a δ function $g_{1D}\delta(x_{i,\ell} - x_{j,\ell})$, where g_{1D} is the two-body interaction parameter given by Astrakharchik *et al.* [70] via

$$g_{1D} = -\frac{2\hbar^2}{ma_{sc}}. \tag{B2}$$

Note that although g_{1D} is negative, it does not yield attraction, which in itself is counterintuitive. As such, the absolute value of g_{1D} is considered in the present calculations.

The interaction strength is defined by the Lieb-Liniger parameter given by $\gamma = mg_{1D}/(\hbar^2 n)$, and from Eq. (B2) this is equivalent to

$$\gamma = -2/(a_{sc}n). \tag{B3}$$

Here $n = \langle N \rangle / L$ is the average linear density of the system, with $\langle N \rangle$ the WAPIMC average particle number. It must be emphasized that γ is varied here by changing n via μ while keeping the scattering length a_{sc} fixed.

APPENDIX C: CORRECTION TO KINETIC ENERGY

According to Ceperley [33], the thermodynamic estimator for the kinetic energy is given by

$$\mathcal{K}_T = \left\langle \frac{3N}{2\tau_0} - \frac{(R_\ell - R_{\ell-1})^2}{4\lambda\tau_0^2} + \frac{\lambda}{\tau_0}\frac{dU^\ell}{d\lambda} \right\rangle, \tag{C1}$$

where $\lambda = \hbar^2/(2m)$. This is the same as E_K [Eq. (15)], except for the correction term, which is the last term on the right-hand side. According to Ceperley, U^ℓ is the total action of a link. However, the WAPIMC code that we obtained from Prokofev [68] does not include this link energy. It makes only use of the kinetic energy in the primitive approximation [Eq. (2.25) in [33]]. Accordingly, we programed $(\lambda/\tau)dU^\ell/d\lambda$ beginning with the pair density matrix ρ given by Eq. (B1). Following Ref. [33], U^ℓ is generally defined by

$$U^\ell \equiv U_2(R_{\ell-1}, R_\ell; \tau_0) = \sum_{i<j} u_2(\vec{r}_{ij,\ell-1}, \vec{r}_{ij,\ell}; \tau_0), \tag{C2}$$

where

$$u_2(\vec{r}_{ij,\ell-1}, \vec{r}_{ij,\ell}; \tau_0) = -\ln \rho(\vec{r}_{ij,\ell-1}, \vec{r}_{ij,\ell}; \tau_0) \tag{C3}$$

and $\vec{r}_{ij,\ell-1} = \vec{r}_{i,\ell-1} - \vec{r}_{j,\ell-1}$ is at time slice $\ell - 1$ whereas $\vec{r}_{ij,\ell}$ is at time slice ℓ. Rewriting Eq. (B1) by substituting $\lambda = \hbar^2/(2m)$, inserting the resulting ρ into (C3) for the 1D case, and evaluating (C2), then differentiating with respect to λ, one arrives at the required correction term at time slice ℓ.

Performing a number of WAPIMC simulations with this new term, it is found that the thermodynamic average $\Delta E_K = \langle(\lambda/\tau)dU/d\lambda\rangle$ with $U = \sum_{\ell=1}^{M} U_2(R_{\ell-1}, R_\ell; \tau_0)$ is quite small, being $\leqslant O(10^{-4})$, as compared to Eq. (15), which is $O(1)$, and therefore ΔE_K is negligible.
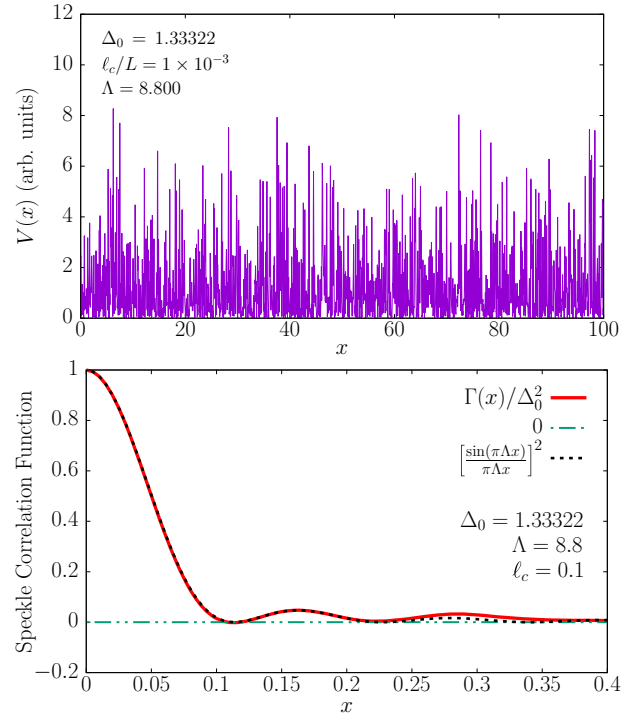

FIG. 8. Top frame: Speckle potential $V(x)$ of length $L = 100$ as generated by the method outlined by Pilati *et al.* [77]. The variance [Eq. (D1)] is $\Delta_0 = 1.333\,22$, ℓ_c is the correlation length, and $\Lambda = 8.8$ is a cutoff momentum [77]. Bottom frame: numerical correlation function of the speckle potential compared to the analytical result $[\sin(\pi\Lambda x)/(\pi\Lambda x)]^2$. The central Gaussian-like peak has a half-width of 0.05 so that $\ell_c = 0.1$ and $\ell_c/\xi_* = 3.542 \times 10^{-2}$. $V(x)$ and Δ_0 are in arbitrary units, whereas ℓ_c and Λ are unitless.

APPENDIX D: SPECKLE POTENTIAL

The speckle potential $V(x)$ used here is displayed in the top frame of Fig. 8. It is the same figure that we used in one of our previous publications [76]. We generated it by a method outlined earlier by Pilati *et al.* [77]. The bottom frame demonstrates the associated numerically obtained correlation function $\Gamma(x)/\Delta_0^2$ compared to the exact analytical result $[\sin(\pi\Lambda x)/(\pi\Lambda x)]^2$. Here $\Lambda \sim 1/\ell_c$ is a cutoff momentum that is related to the correlation length ℓ_c of the speckle potential, and Δ_0 is the variance of the latter given by

$$\Delta_0 = (\langle V^2 \rangle - \langle V \rangle^2)^{1/2}. \tag{D1}$$

Here

$$\langle \cdots \rangle = \frac{1}{L} \int_0^L (\cdots) dx, \tag{D2}$$

so that $(\cdots)$ is either $V(x)$ or $V^2(x)$, where $\langle V \rangle$ represents the strength of the speckle potential, and L is the length of the system. It should be noted that $\langle V(x) \rangle \neq 0$ in order to account for the effects of a shift in the chemical potential. The half-width at half-maximum of the Gaussian-like peak of $\Gamma(x)/\Delta_0^2$ centered around the origin in the bottom frame is 0.05 and therefore $\ell_c = 0.1$. The ratios ℓ_c/L and ℓ_c/ξ_* are much smaller than 1, where $L = 100$, and ξ_* is the localization

TABLE I. Comparisons between the WAPIMC kinetic energies E_K [Eq. (15)] obtained with the single speckle realization of this work and from an ensemble average $\langle E_K \rangle_{\text{ens}}$ over 30 realizations of different speckle potentials, all being of the same length $L/\ell_c = 1000$. From left to right, the table lists the chemical potential μT_d, temperature T/T_d, scattering length a_{sc}/ℓ_c, speckle strength $\langle V \rangle$, E_K, and $\langle E_K \rangle_{\text{ens}}$.

μT_d	T (T_d)	a_{sc} (ℓ_c)	$\langle V \rangle$ (δV_0)	E_K (T_d) one real.	$\langle E_K \rangle_{\text{ens}}$ (T_d) sev. real.
20	0.200	10	20	0.2985 ± 0.0051	0.2683 ± 0.0094
40	0.400	10	20	0.2390 ± 0.0069	0.2271 ± 0.0107

length given by [18]

$$\xi_* = \left[\frac{\hbar^4}{\Delta_0^2 m^2 \ell_c} \right]^{1/3}, \tag{D3}$$

with m the mass of a boson. The speckle potential is generated numerically external to the WAPIMC code. It is uploaded into the latter, and its strength is controlled by a multiplicative factor f, that is, $\Delta_0 \to f\Delta_0$.

The speckle potential arises from just one disorder realization. Because our system size is much larger than the speckle correlation length, i.e., $L/\ell_c = 1000$, the disorder potential and the associated physical quantities are self-averaging. Clement *et al.* [78] discussed the self-averaging properties of a speckle pattern. By defining the first and second moments of the ensemble-averaged speckle potential, they determined associated standard deviations, $\sigma_{m_1}(d)$ and $\sigma_{m_2}(d)$, respectively. In the asymptotic limit $d \gg \Delta z$ they displayed the expression [their Eq. (7)]

$$\frac{\sigma_{m_2}(d)}{\sigma_{m_2}(0)} \approx 0.959 \sqrt{\frac{\Delta z}{d}}, \tag{D4}$$

where d is the length of the system and Δz is the speckle correlation length. In the present work, $d/\Delta z = 1000$ and therefore $\sigma_{m_2}(100)/\sigma_{m_2}(0) \approx 0.03$. Indeed, it has been argued that when (D4) tends to zero, the system becomes self-averaging.

Moreover, in order to provide further proof for the self-averaging property of the speckle potential $V(x)$ applied in this work, we generated 30 different other realizations of $V(x)$ of the same size L, and we evaluated ensemble averages of the kinetic energy, $\langle E_K \rangle_{\text{ens}}$, over the realizations of the speckle potential. This has been done for two arbitrarily chosen specimens of the present work at the parameters indicated in Table I. It turns out that the corresponding values of E_K, using the single speckle realization described above, are very close indeed to $\langle E_K \rangle_{\text{ens}}$, and they lie within the range specified by the error bars.

APPENDIX E: CURRENT-CURRENT CORRELATION FUNCTION

In this Appendix, it is shown that the current-current correlation function

$$C(\tau) = \int_0^\beta \langle J(\tau)J(0) \rangle d\tau \sim \langle W \rangle^2, \tag{E1}$$

where W is the winding number (10) and $J(\tau)$ is the time-dependent current at time τ. In WAPIMC, the current is

evaluated via

$$J(\tau) \to J_\ell = \sum_{i=1}^N v_{i,\ell}, \tag{E2}$$

where

$$v_{i,\ell} = \frac{x_{i,\ell} - x_{i,\ell-1}}{\tau_0} \tag{E3}$$

is the "velocity" of particle "i" at time ℓ. In a Monte Carlo evaluation of the integral of $J(\tau)J(0)$ at each WAPIMC configuration, that is,

$$\int_0^\beta J(\tau)J(0)d\tau = \tau_0 \sum_{\ell=1}^M \sum_{n=1}^M J_{\ell+n} J_\ell$$

$$= \tau_0 \sum_{\ell=1}^M \left\{ \sum_{n=1}^M \left[\sum_{i=1}^N \left(\frac{x_{i,n+\ell} - x_{i,n+\ell-1}}{\tau_0} \right) \right. \right.$$

$$\left. \left. \times \sum_{j=1}^N \left(\frac{x_{j,\ell} - x_{j,\ell-1}}{\tau_0} \right) \right] \right\},$$

one can separate the $n = 0$ terms from all the other terms to get

$$\sum_{\ell=1}^M \sum_{n=1}^M J_{\ell+n} J_\ell = \sum_{\ell=1}^M J_\ell^2 + \sum_{k \neq \ell}^M J_k J_\ell, \tag{E4}$$

the first term on the right-hand side being related to the winding number W. This can be seen by making the expansion

$$\sum_{\ell=1}^M J_\ell^2 = \left[\sum_{\ell=1}^M J_\ell \right]^2 - \sum_{k \neq \ell}^M J_\ell J_k$$

$$= \frac{L^2 W^2}{\tau_0^2} - \sum_{k \neq \ell}^M J_\ell J_k, \tag{E5}$$

and substituting (E5) back into (E4) as a result of which the $k \neq \ell$ terms cancel out so that

$$\int_0^\beta J(\tau)J(0)d\tau = \tau_0 \sum_{\ell=1}^M \sum_{n=1}^M J_{\ell+n} J_\ell = \frac{L^2 W^2}{\tau_0}. \tag{E6}$$

Consequently, $C(\tau)$ is zero because $\langle W^2 \rangle$ in the current system is always zero and therefore provides us with no further information.

[1] T. Roscilde, Phys. Rev. A **77**, 063605 (2008).

[2] T. Paul, P. Schlagheck, P. Leboeuf, and N. Pavloff, Phys. Rev. Lett. **98**, 210602 (2007).

[3] L. Sanchez-Palencia, D. Clément, P. Lugan, P. Bouyer, G. V. Shlyapnikov, and A. Aspect, Phys. Rev. Lett. **98**, 210401 (2007).

[4] P. Lugan, D. Clément, P. Bouyer, A. Aspect, and L. Sanchez-Palencia, Phys. Rev. Lett. **99**, 180402 (2007).

[5] J. Radić, V. Bačić, D. Jukić, M. Segev, and H. Buljan, Phys. Rev. A **81**, 063639 (2010).

[6] J. C. C. Cestari, A. Foerster, and M. A. Gusmão, Phys. Rev. A **82**, 063634 (2010).

[7] J. Billy, V. Josse, Z. Zuo, A. Bernard, B. Hambrecht, P. Lugan, D. Clément, L. Sanchez-Palencia, P. Bouyer, and A. Aspect, Nature **453**, 891 (2008).

[8] R. Vosk and E. Altman, Phys. Rev. B **85**, 024531 (2012).

[9] Z. Ristivojevic, A. Petković, P. Le Doussal, and T. Giamarchi, Phys. Rev. B **90**, 125144 (2014).

[10] E. Altman, Y. Kafri, A. Polkovnikov, and G. Refael, Phys. Rev. B **81**, 174528 (2010).

[11] T. Giamarchi and H. J. Schulz, Europhys. Lett. **3**, 1287 (1987).

[12] T. Giamarchi and H. J. Schulz, Phys. Rev. B **37**, 325 (1988).

[13] P. Lugan, D. Clément, P. Bouyer, A. Aspect, M. Lewenstein, and L. Sanchez-Palencia, Phys. Rev. Lett. **98**, 170403 (2007.

[14] G. Roux, T. Barthel, I. P. McCulloch, C. Kollath, U. Schollwöck, and T. Giamarchi, Phys. Rev. A **78**, 023628 (2008).

[15] L. Fontanesi, M. Wouters, and V. Savona, Phys. Rev. Lett. **103**, 030403 (2009).

[16] L. Fontanesi, M. Wouters, and V. Savona, Phys. Rev. A **83**, 033626 (2011).

[17] V. P. Michal, I. L. Aleiner, B. L. Altshuler, and G. V. Shlyapnikov, Proc. Natl. Acad. Sci. (USA) **113**, E4455 (2016).

[18] I. L. Aleiner, B. L. Altshuler, and G. V. Shlyapnikov, Nat. Phys. **6**, 900 (2010).

[19] L. Gori, T. Barthel, A. Kumar, E. Lucioni, L. Tanzi, M. Inguscio, G. Modugno, T. Giamarchi, C. D'Errico, and G. Roux, Phys. Rev. A **93**, 033650 (2016).

[20] H. Yao, T. Giamarchi, and L. Sanchez-Palencia, Phys. Rev. Lett. **125**, 060401 (2020).

[21] M. Schreiber, S. S. Hodgman, P. Bordia, H. P. Lüschen, M. H. Fischer, R. Vosk, E. Altman, U. Schneider, and I. Bloch, Science **349**, 842 (2015).

[22] E. Akkermans, S. Ghosh, and Z. H. Musslimani, J. Phys. B **41**, 045302 (2008).

[23] G. Modugno, Rep. Prog. Phys. **73**, 102401 (2010).

[24] L. Sanchez-Palencia and M. Lewenstein, Nat. Phys. **6**, 87 (2010).

[25] R. T. Scalettar, G. G. Batrouni, and G. T. Zimanyi, Phys. Rev. Lett. **66**, 3144 (1991).

[26] K. G. Singh and D. S. Rokhsar, Phys. Rev. B **46**, 3002 (1992).

[27] L. Zhang and M. Ma, Phys. Rev. B **45**, 4855 (1992).

[28] G. Masella, N. V. Prokofev, and G. Pupillo, Nat. Commun. **13**, 2113 (2022).

[29] N. V. Prokofev, B. V. Svistunov, and I. S. Tupitsyn, J. Exp. Theor. Phys. **87**, 310 (1998).

[30] A. Del Maestro and I. Affleck, Phys. Rev. B **82**, 060515(R) (2010).

[31] L. Vranješ Markić, H. Vrcan, Z. Zuhrianda, and H. R. Glyde, Phys. Rev. B **97**, 014513 (2018).

[32] A. Del Maestro, M. Boninsegni, and I. Affleck, Phys. Rev. Lett. **106**, 105303 (2011).

[33] D. M. Ceperley, Rev. Mod. Phys. **67**, 279 (1995).

[34] A. R. Sakhel, Phys. Rev. A **94**, 033622 (2016).

[35] M. P. A. Fisher, P. B. Weichman, G. Grinstein, and D. S. Fisher, Phys. Rev. B **40**, 546 (1989).

[36] C. Meldgin, U. Ray, P. Russ, D. Chen, D. M. Ceperley, and B. DeMarco, Nat. Phys. **12**, 646 (2016).

[37] O. A. Rodríguez-López, M. A. Solís, and J. Boronat, Phys. Rev. A **103**, 013311 (2021).

[38] M. Snoek, Phys. Rev. A **85**, 013635 (2012).

[39] A. Rançon and N. Dupuis, Phys. Rev. A **86**, 043624 (2012).

[40] S. Konabe, T. Nikuni, and M. Nakamura, Phys. Rev. A **73**, 033621 (2006).

[41] M. Boninsegni, N. V. Prokof'ev, and B. V. Svistunov, Phys. Rev. E **74**, 036701 (2006).

[42] V. P. Michal, B. L. Altshuler, and G. V. Shlyapnikov, Phys. Rev. Lett. **113**, 045304 (2014).

[43] I. V. Gornyi, A. D. Mirlin, and D. G. Polyakov, Phys. Rev. Lett. **95**, 206603 (2005).

[44] Y. P. Chen, J. Hitchcock, D. Dries, M. Junker, C. Welford, and R. G. Hulet, Phys. Rev. A **77**, 033632 (2008).

[45] L. Fontanesi, M. Wouters, and V. Savona, Phys. Rev. A **81**, 053603 (2010).

[46] D. Clément, A. F. Varón, M. Hugbart, J. A. Retter, P. Bouyer, L. Sanchez-Palencia, D. M. Gangardt, G. V. Shlyapnikov, and A. Aspect, Phys. Rev. Lett. **95**, 170409 (2005).

[47] C. Fort, L. Fallani, V. Guarrera, J. E. Lye, M. Modugno, D. S. Wiersma, and M. Inguscio, Phys. Rev. Lett. **95**, 170410 (2005).

[48] T. Schulte, S. Drenkelforth, J. Kruse, W. Ertmer, J. Arlt, K. Sacha, J. Zakrzewski, and M. Lewenstein, Phys. Rev. Lett. **95**, 170411 (2005).

[49] T. Schulte, S. Drenkelforth, J. Kruse, R. Tiemeyer, K. Sacha, J. Zakrzewski, M. Lewenstein, W. Ertmer, and J. J. Arlt, New J. Phys. **8**, 230 (2006).

[50] L. Sanchez-Palencia, Phys. Rev. A **74**, 053625 (2006).

[51] L. Sanchez-Palencia, D. Clément, P. Lugan, P. Bouyer, and A. Aspect, New J. Phys. **10**, 045019 (2008).

[52] T. Paul, M. Albert, P. Schlagheck, P. Leboeuf, and N. Pavloff, Phys. Rev. A **80**, 033615 (2009).

[53] M. Albert, T. Paul, N. Pavloff, and P. Leboeuf, Phys. Rev. A **82**, 011602(R) (2010).

[54] S. S. Kondov, W. R. McGehee, W. Xu, and B. DeMarco, Phys. Rev. Lett. **114**, 083002 (2015).

[55] I. V. Gornyi, A. D. Mirlin, and D. G. Polyakov, Phys. Rev. B **75**, 085421 (2007).

[56] C. L. Kane and M. P. A. Fisher, Phys. Rev. Lett. **68**, 1220 (1992).

[57] M. Ogata and H. Fukuyama, Phys. Rev. Lett. **73**, 468 (1994).

[58] E. Levy, A. Tsukernik, M. Karpovski, A. Palevski, B. Dwir, E. Pelucchi, A. Rudra, E. Kapon, and Y. Oreg, Phys. Rev. Lett. **97**, 196802 (2006).

[59] I. Amanatidis, I. Kleftogiannis, F. Falceto, and V. A. Gopar, Phys. Rev. B **85**, 235450 (2012).

[60] E. L. Pollock and D. M. Ceperley, Phys. Rev. B **30**, 2555 (1984).

[61] G. G. Batrouni and R. T. Scalettar, Phys. Rev. B **46**, 9051 (1992).

[62] J. E. Hirsch, R. L. Sugar, D. J. Scalapino, and R. Blankenbecler, Phys. Rev. B **26**, 5033 (1982).

[63] M. Barma and B. S. Shastry, Phys. Rev. B **18**, 3351 (1978).

[64] J. Hubbard, Phys. Rev. Lett. **3**, 77 (1959).

[65] H. Steinberg, O. M. Auslaender, A. Yacoby, J. Qian, G. A. Fiete, Y. Tserkovnyak, B. I. Halperin, K. W. Baldwin, L. N. Pfeiffer, and K. W. West, Phys. Rev. B **73**, 113307 (2006).

[66] C. Kittel, *Introduction to Solid State Physics*, 8th ed. (Wiley, New Jersey, 2005).

[67] F. J. Schupp, M. M. Mirza, D. A. MacLaren, G. A. D. Briggs, D. J. Paul, and J. A. Mol, Phys. Rev. B **98**, 235428 (2018).

[68] N. Prokofev, UMASS Amherst, 2013 (private communication).

[69] B. V. Svistunov, E. S. Babaev, and N. V. Prokof'ev, *Superfluid States of Matter* (CRC, Boca Raton, FL, 2015).

[70] G. E. Astrakharchik, J. Boronat, J. Casulleras, and S. Giorgini, Phys. Rev. Lett. **95**, 190407 (2005).

[71] E. Rabani, D. R. Reichman, G. Krilov, and B. J. Berne, Proc. Natl. Acad. Sci. (USA) **99**, 1129 (2002).

[72] A. R. Sakhel, Eur. Phys. J. D **66**, 267 (2012).

[73] N. Cherroret, T. Karpiuk, B. Grémaud, and C. Miniatura, Phys. Rev. A **92**, 063614 (2015).

[74] K. Nikolić and A. MacKinnon, Phys. Rev. B **50**, 11008 (1994).

[75] R. P. Feynman, *Statistical Mechanics* (Westview, Advanced Book Program, Boulder, CO, 1998).

[76] R. R. Sakhel and A. R. Sakhel, J. Phys.: Condens. Matter **32**, 315401 (2020).

[77] S. Pilati, S. Giorgini, M. Modugno, and N. Prokof'ev, New J. Phys. **12**, 073003 (2010).

[78] D. Clément, A. F. Varón, J. A. Retter, L. Sanchez-Palencia, A. Aspect, and P. Bouyer, New J. Phys. **8**, 165 (2006).